Electronic Supplementary Material (ESI) for Nanoscale.

Supporting Information

Water structure, dynamics and reactivity on a TiO_2-nanoparticle surface: New insigths from ab initio molecular dynamics

Fredrik Grote and Alexander P. Lyubartsev*

Department of Materials and Environmental Chemistry, Stockholm University,

SE 106 91, Stockholm, Sweden

tel. +46-8161193

E-mail: alexander.lyubartsev@mmk.su.se

S1. Convergence of plane-wave cutoff and mapping of gaussians onto multigrid

In DFT calculations using the GPW method as implemented in the CP2K software orbitals are expanded in a contracted gaussian basis set. In addition, this method also uses a representation of the electron density in an auxillary plane wave basis set. The code represents gaussian functions on a multigrid in order for functions with different width to be covered by roughly the same number of grid points. Two key parameters in these calculations are the plane wave cutoff for the finest grid level (CUTOFF) and the plane wave cutoff for the reference grid (REL_CUTOFF). A gaussian gets mapped onto the coarsest level of the multigrid on which the number of grid points covered by the function is greater than or equal to the number of grid points covered by a guassian with unit standard deviation on the reference grid. Following the procedure described in the CP2K tutorial (https://www.cp2k.org/howto:converging_cutoff) we computed single point energies for a system snapshot with CUTOFF ranging from 50 to 500 Ry keeping REL_CUTOFF fixed at 70 Ry. Figure S1 (a) shows the convergence of the single point energy as function of CUTOFF parameter and shows that the energy converges at CUTOFF equal to 200 Ry. This also gives a uniform distribution over the different levels of the multigrid as illustrated in Figure S2 showing the number of gaussians mapped to the different levels of the multigrid as function of the plane wave cutoff. Then REL_CUTOFF parameter was varied keeping CUTOFF fixed at 200 Ry. Figure S1 (b) shows that the energy converged within 30 Ry. This gives confidence for choosing CUTOFF to be 200 Ry and REL_CUTOFF equal to 30 Ry.

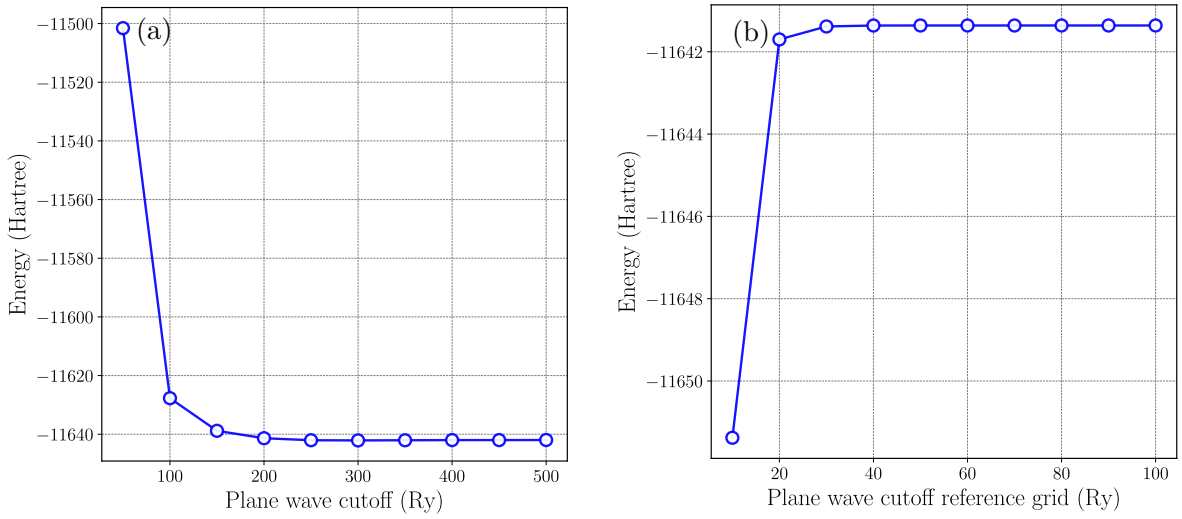

Figure S1: Convergence of energy with respect to (a) REL_CUTOFF and (b) CUTOFF.

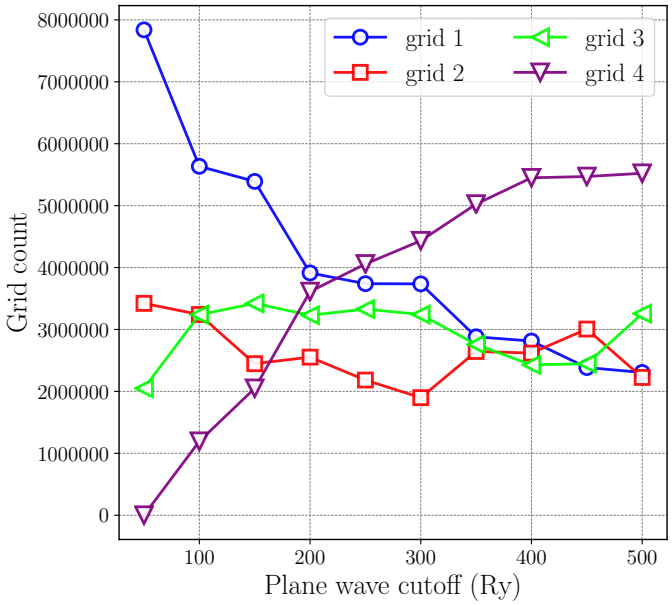

Figure S2: Number of gaussians mapped onto the different levels of the multigrid.

S2. Equilibration

Equilibration of the simulated system was monitored by checking how properties were changing as function of the simulation time. Figure S3 shows potential energy and temperature as function of simulation time during the equilibration phase of the simulation and shows that these properties became stable within the first picosecond of the simulation, with a slight drift lasting 2-3 ps. RMSD of the nanoparticle atoms relative to the initial configuration shows that it does not undergo significant sturctural changes, see Figure S4. Equilibration of the overall structure was analyzed by monitoring convergence of the Ti-O RDF shown in Figure S5. The RDF also converges within the first picosecond of the simulation suggesting that the system is equilibrated after this time. In order to check convergence of structure at the TiO_2-water interface we also computed the RDF between atom type O_{2c}-H in five different 9 ps windows, see Figure S6. The result shows that the surface structure is the same in the different time windows apart from the appearance of a peak around 1 Å in window 4 and 5 due to dissociation of water discussed in the main text.

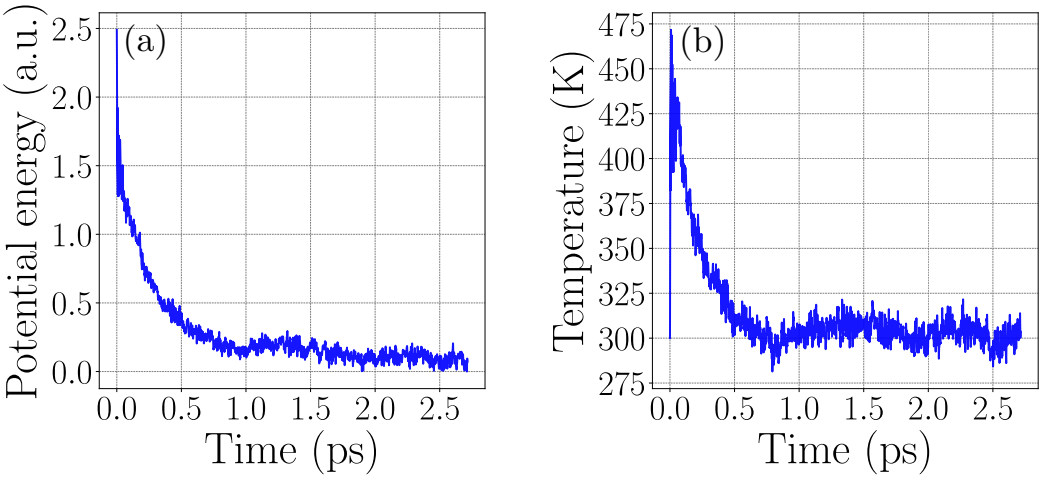

Figure S3: Properties as function of simulation time during equilibration (a) potential energy and (b) temperature.

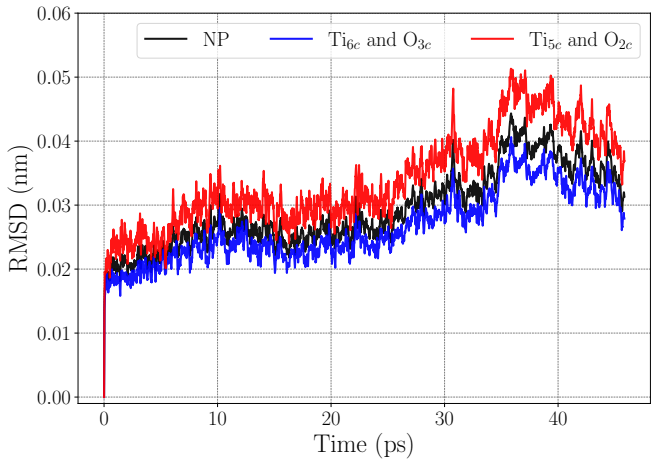

Figure S4: RMSD from starting configuration for all atoms in nanoparticle (NP), and taken separately for atoms on the surface (Ti_{5c}, O_{2c}) and atoms in the interior of the nanoparticle (Ti_{6c}, O_{3c}).

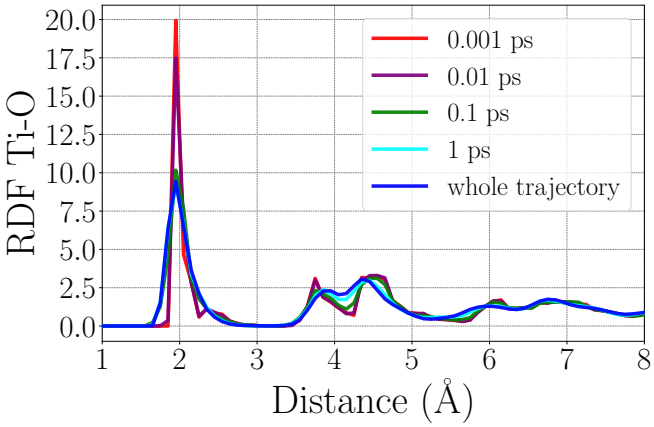

Figure S5: Convergence of Ti-O RDF.

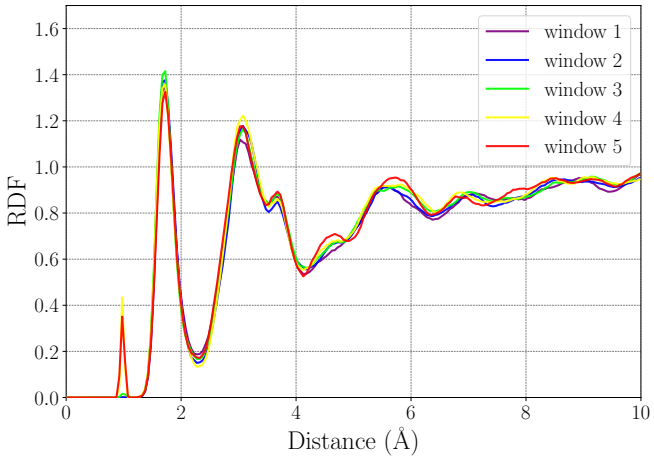

Figure S6: RDF computed between atom types O_{2c}-H in five different 9 ps windows.

S3. Distribution of net atomic charges

Figure S7 shows the distribution of net atomic charges for atoms assigned to different atom types.

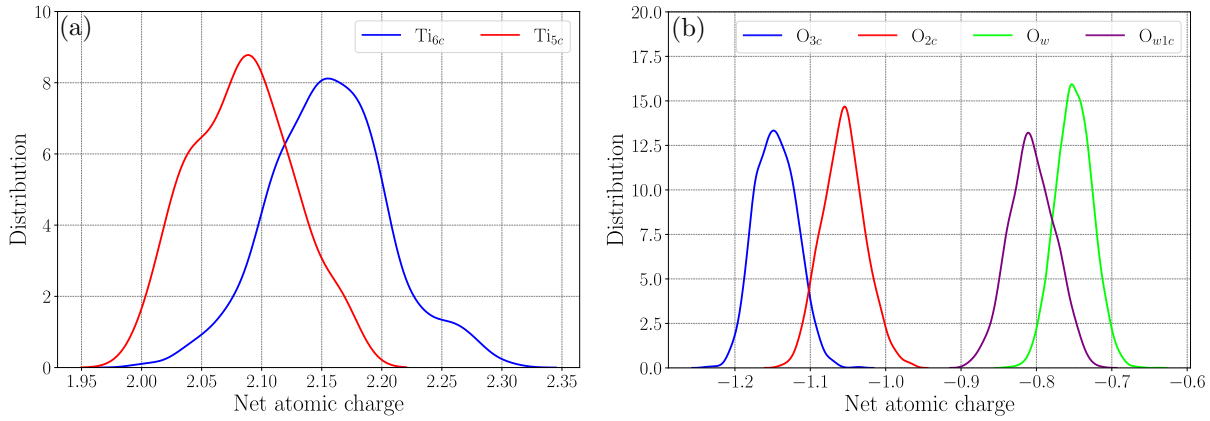

Figure S7: Distribution of net atomic charges (a) titanium atom types (b) oxygen atom types.

S4. Radial distribution functions

In Figure S8 RDFs between water oxygen atoms and oxygen atoms in the nanoparticle are shown. Figure S9 and S10 show RDFs computed between titanium atom types and oxygen atom types in water and the nanoparticle, respectively.

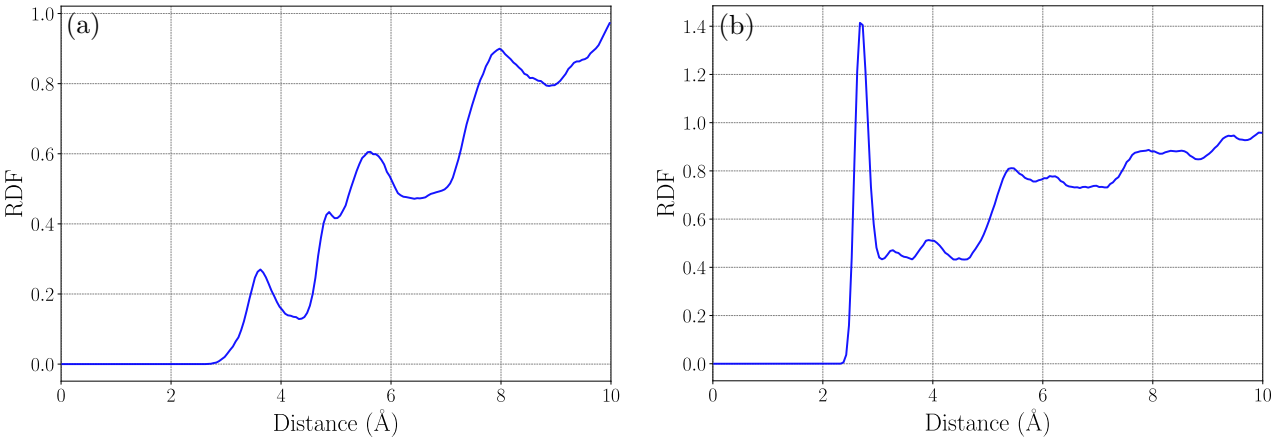

Figure S8: Oxygen-oxygen RDFs between atom types (a) O_w-O_{3c}, (b) O_w-O_{2c}.

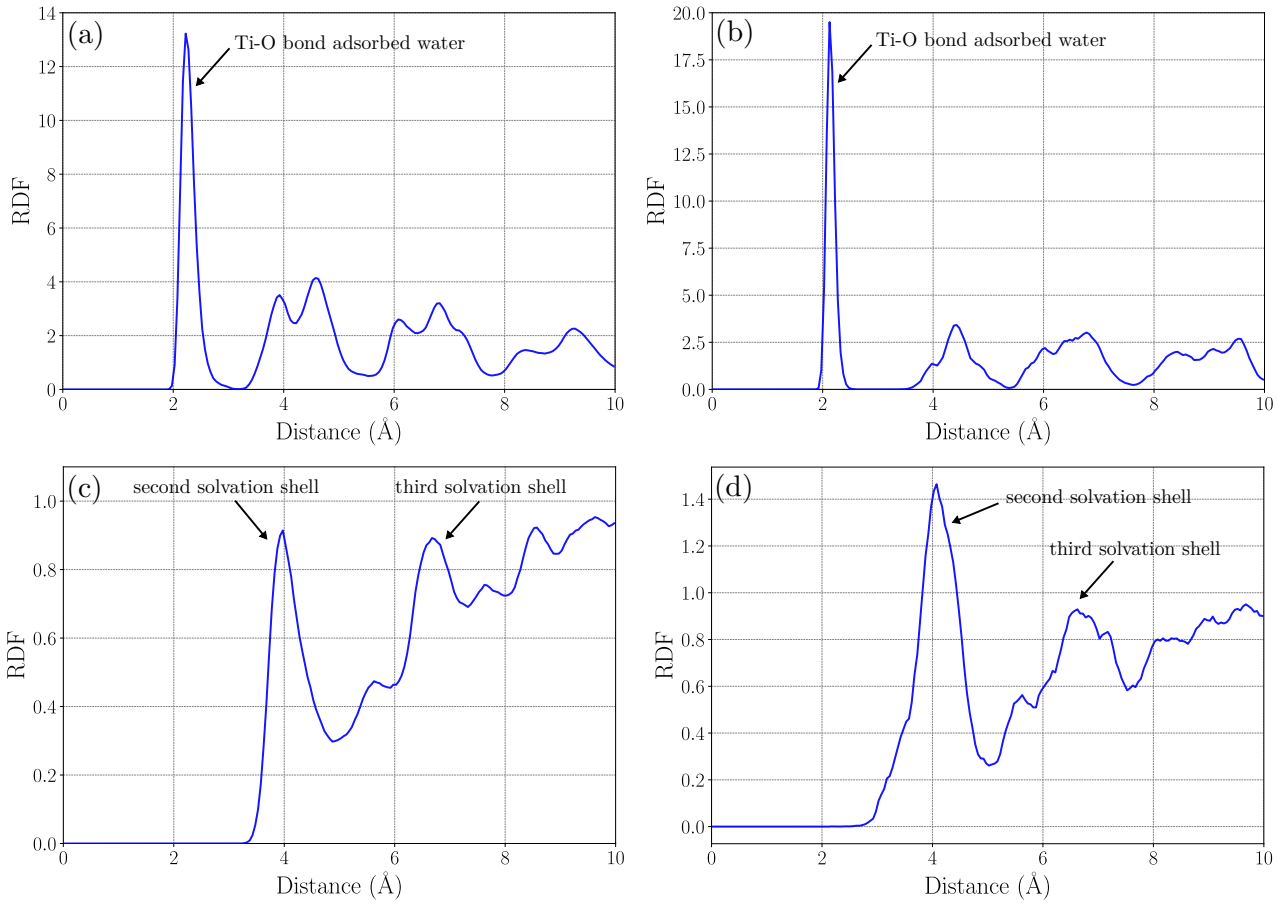

Figure S9: Titanium-oxygen RDFs between atom types (a) Ti_{6c}-O_{w1c}, (b) Ti_{5c}-O_{w1c} (c), Ti_{6c}-O_w and (d) Ti_{5c}-O_w.

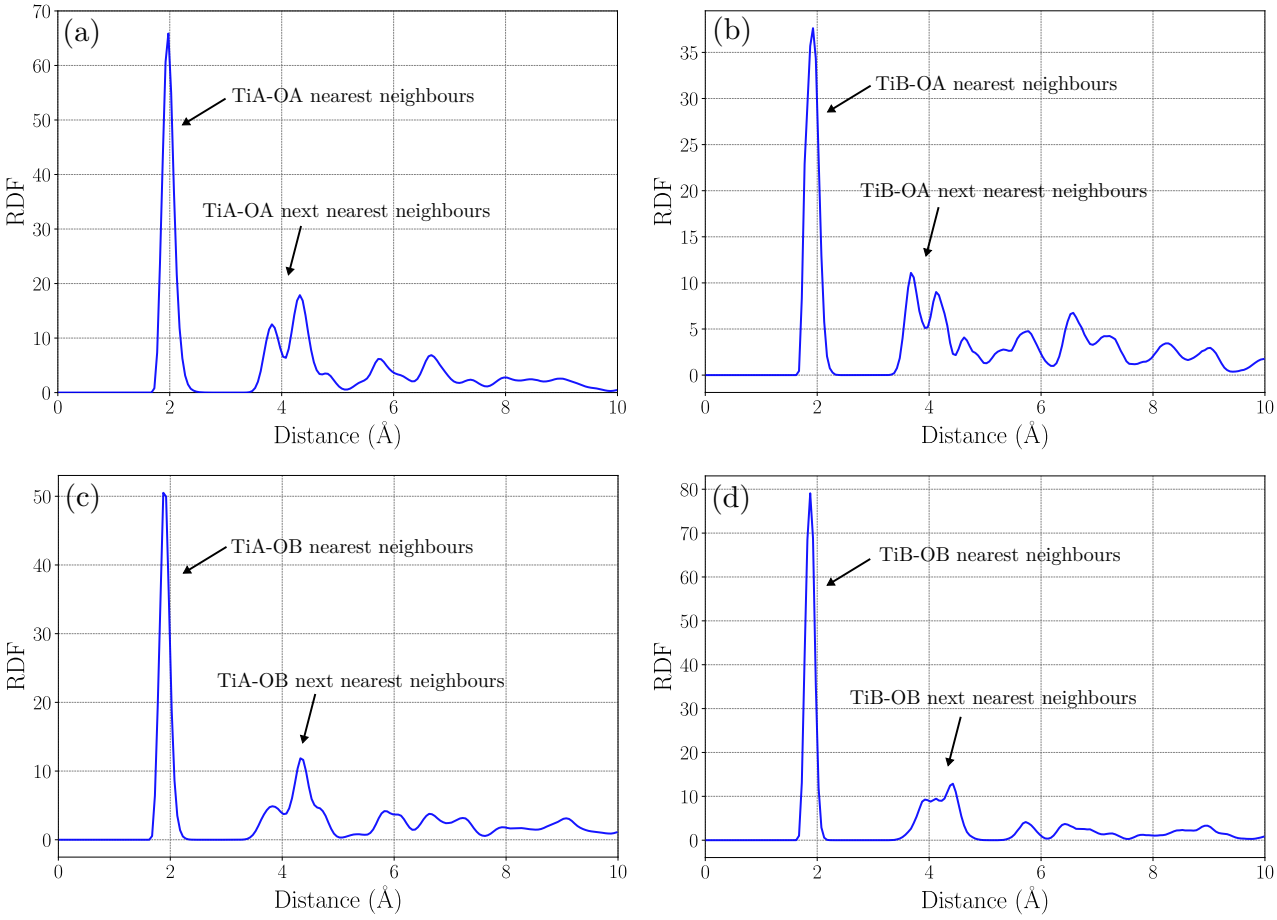

Figure S10: Titanium-oxygen RDFs in nanoparticle between atom types (a) TiA-OA (b) TiB-OA (c) TiA-OB and (d) TiB-OB.

S5. Bond order

Although interatomic distances can provide valuable information about reaction pathways they do not unambiguously quantify the amount of covalent interaction between pairs of atoms. For this reason we also calculated bond orders using the chargemol software for bonds O75-H948 and O430-H431 for a set of snapshots extracted from the water splitting. The result shown in Figure S11 confirms that water splitting occurs by the mechanism described in the main text. For snapshot 1,2 and 5 bond order was computed from not fully converged electron density which can effect the result.

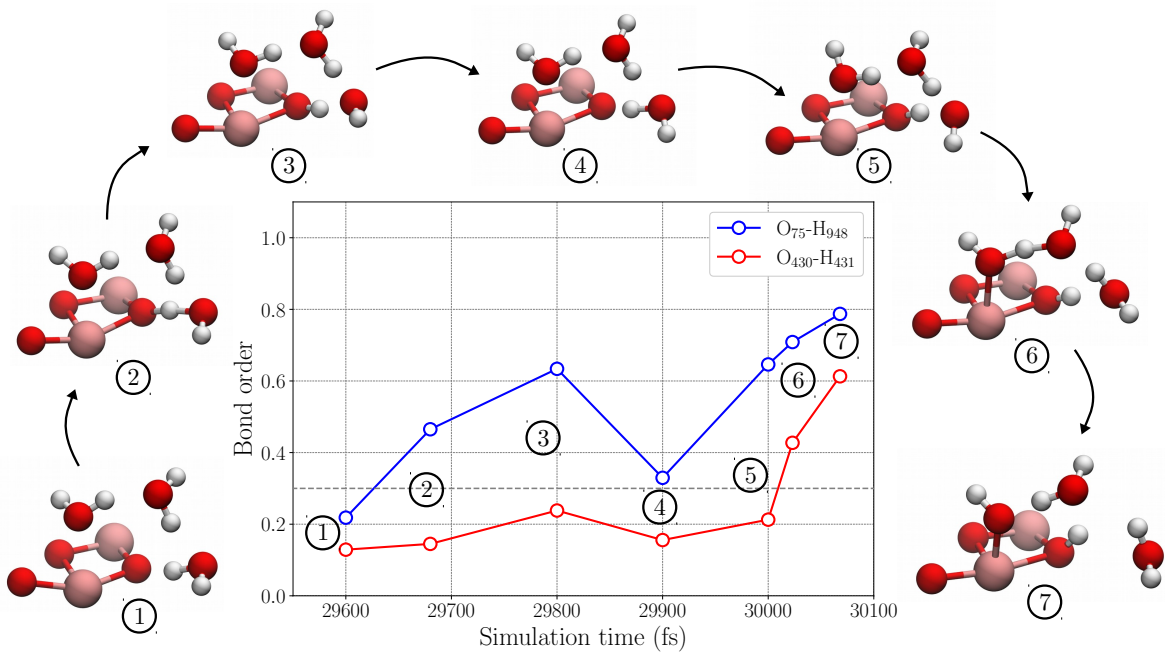

Figure S11: Bond order as function of time during water splitting reaction for bonds between O75-H948 and O430-H431. The grey dashed line at bond order equal to 0.3 indicates a threshold for covalent bonding.

S6. Distribution of reaction coordinates during water splitting

Distribution of two reaction coordinates during water splitting (1) donor-acceptor distance and (2) $\delta = R_{A-H} - R_{D-H}$ where R_{A-H} is the distance between the proton and the acceptor atom and R_{D-H} is the distance between the proton and the donor atom.

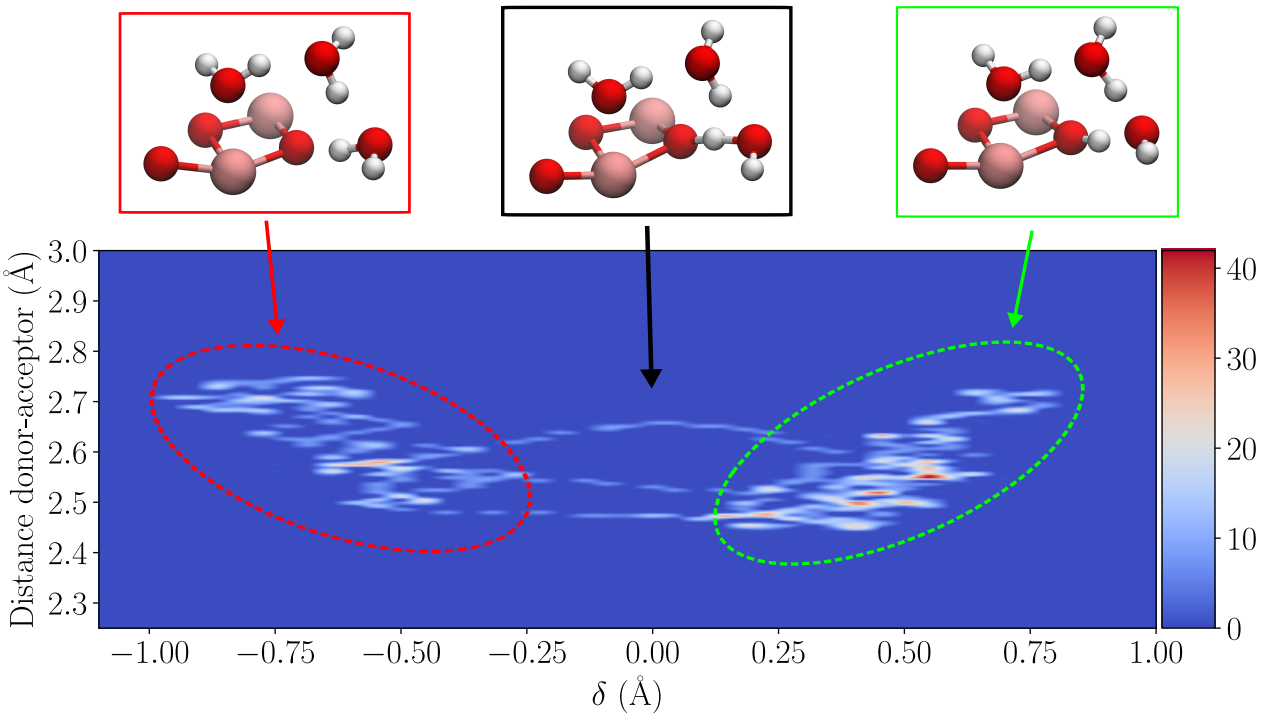

Figure S12: Distribution of δ and acceptor-donor distance during water dissociation.

S7. Water adsorption/desorption equilibrium

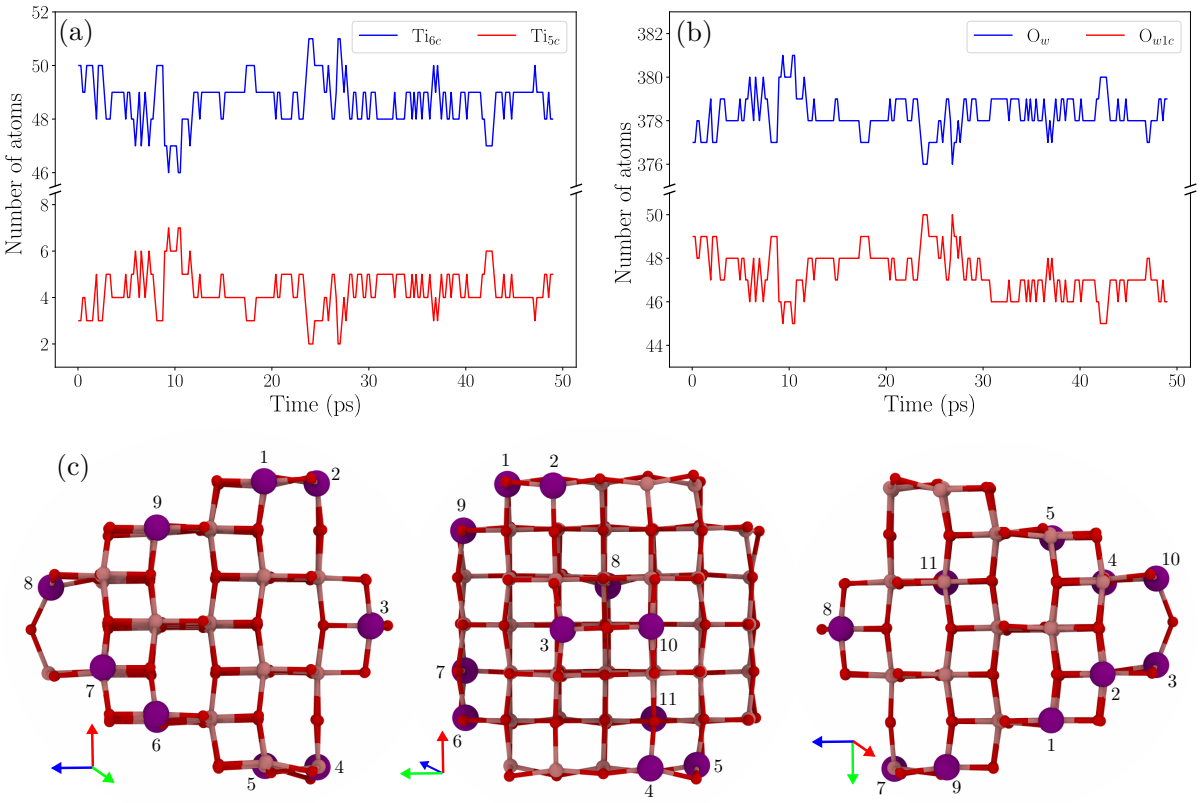

Figure S13: Time evolution of the number of atoms belonging to types (a) Ti_{6c} and Ti_{5c}, (b) O_w and O_{w1c} and (c) visualization of nanoparticle from three different orientations with Ti-atoms changing type between Ti_{6c} and Ti_{5c} labeled as 1-11 and shown in purple colour.

S8. Reorientational time correlation functions

In order to further analyse if reorientation of water molecules is faster in the L_1 layer than in L_2 we computed the TCF of the second order Legendre polynomial for three orthogonal vectors in the water molecule. The result shown in Figure S14 confirms that water molecules reorient faster in the L_1 layer compared to L_2 for all three vectors.

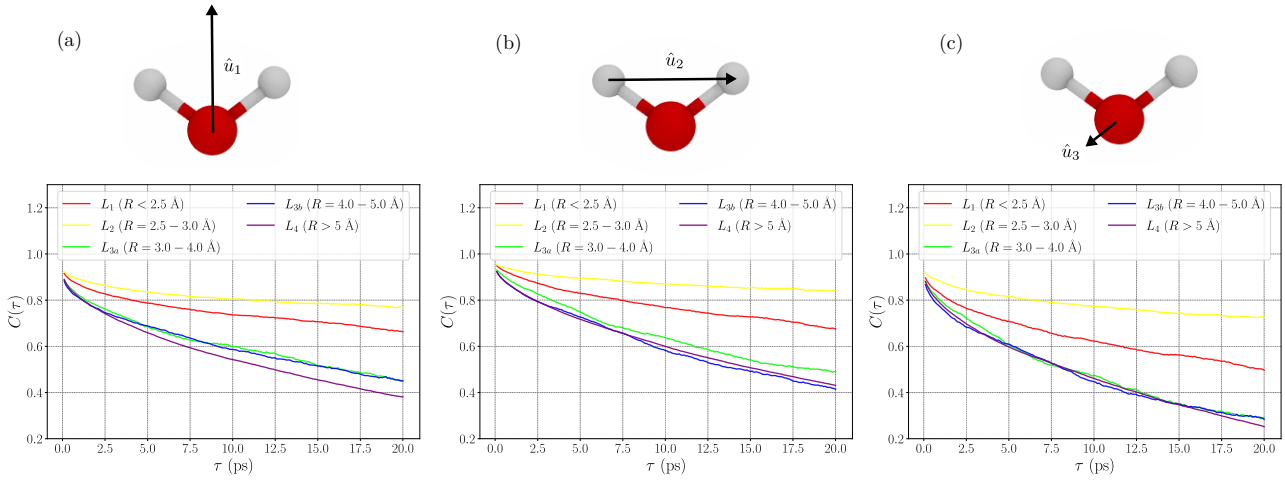

Figure S14: TCFs of second Legendre polynomial for three orthogonal vectors in the water molecule (a) vector along HOH bisector, (b) vector along HH separation and (c) vector orthogonal to the HOH plane.

S9. Diffusion

Figure S15 shows the water diffusion coefficient as function of the distance from the nanoparticle surface where R is the minimum distance from the water oxygen atom to any atom in the nanoparticle.

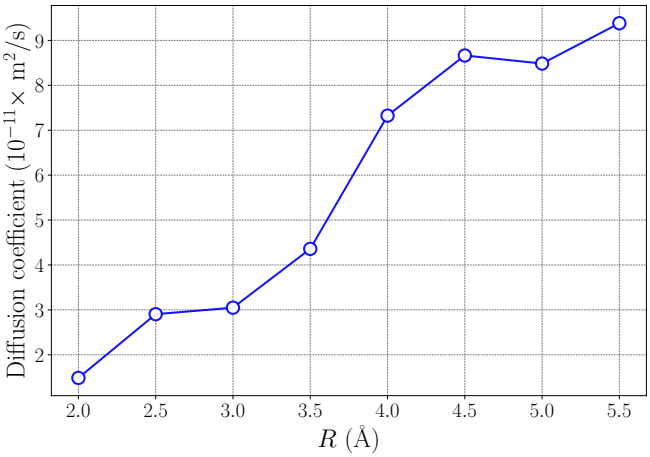

Figure S15: Diffusion coefficient as function of distance from the surface.